# Supporting Information

# Porphyrin Bridged SnO$_2$/Active layer for Efficient and Stable Inverted Organic Solar Cells

*Jifa Wu,[a] Lihua Meng,[a] Yumeng Li,[a] Xinkang Wang,[a] Feng Tang,[b] Yinchun Guo,[a] Ting Wang,[a] Yuang Fu,[c] Xinhui Lu,[c] Baobing Fan,[a] Junwu Chen[a] and Xiaobin Peng*[a]*

[a] State Key Laboratory of Luminescent Materials and Devices, Institute of Polymer Optoelectronic Materials and Devices, Guangdong Basic Research Center of Excellence for Energy and Information Polymer Materials, South China University of Technology, 381 Wushan Road, Guangzhou, 510640, China

[b] International Collaborative Laboratory of 2D Materials for Optoelectronics Science and Technology of Ministry Education, Institute of Microscale Optoelectronics, Shenzhen University, Shenzhen 518060, P. R. China

[c] Department of Physics, The Chinese University of Hong Kong, New Territories, Hong Kong 999077, China

E-mail address: chxbpeng@scut.edu.cn.

# 1. Experimental Section

## 1.1. Materials

Indium tin oxide (ITO) glass (surface resistance is 15 Ω·sq-1, light transmission is 88%, glass thickness is 0.7mm, ITO thickness is 135nm) was purchased from Wuhu Jing Hui Co., Ltd. China. Poly(1-(5-(4,8-bis(5-(2-ethylhexyl)-4-fluorothiophen-2-yl)benzo[1,2-b:4,5-b']dithiophen-2-yl)thiophen-2-yl)-5,7-bis(2-ethylhexyl)-3-(thiophen-2-yl)-4H,8H-benzo[1,2-c:4,5-c']dithiophene-4,8-dione) (PM6), L8-BO and BTP-eC9 were purchased from Solamer. Chloroform (CF), 1-Chloronaphthalene (CN) and 1,8-diiodooctane (DIO) were all purchased from TCI. $SnO_2$ colloidal aqueous solution was purchased from Sigma-Aldrich (China) with a concentration of 15 wt%. TPP-OEG was synthesized in our laboratory. Unless otherwise noted, they were all used without further purification.

## Synthesis of TPP-OEG

All compounds and solvents were purchased from commercial sources (Aldrich, JK Chemical and or TCI) and used as received unless otherwise indicated. Column chromatography with 200-300 mesh silica was used to purify the compounds. All manipulations involving air-sensitive reagents were performed under an atmosphere of dry argon.
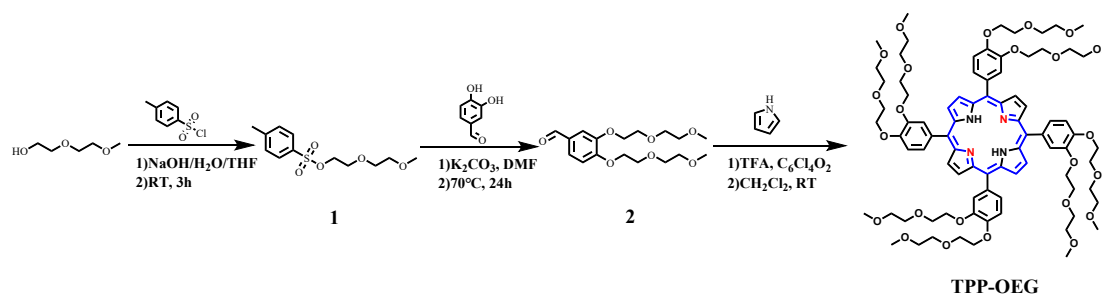


Scheme S1. Synthetic route of the TPP-OEG.

2-(2-Methoxyethoxy)ethyl p-Toluenesulfonate (1):

Sodium hydroxide (NaOH, 2.40 g, 0.060 mol) was dissolved in 15 mL deionized water. Diethylene glycol monomethyl ether (3.67 g, 30.5 mmol) was dissolved in 10 mL tetrahydrofuran (THF). After complete dissolution, the aqueous NaOH solution and the

THF solution were combined and cooled to 0 °C. A separate solution of p-toluenesulfonyl chloride (4-methylbenzene-sulfonyl chloride, 5.82 g, 30.5 mmol) in 15 mL THF was added dropwise over 30 minutes to the cold mixture, maintaining the temperature between 0 and 5 °C. After the addition was complete, the reaction was stirred at room temperature for 3 h. The reaction mixture was then quenched with ice water and extracted with dichloromethane (DCM). The combined organic phases were dried over anhydrous $Na_2SO_4$, filtered, and evaporated under reduced pressure. The residue was obtained as a colorless oil in 98% yield. ^{1}H NMR (500 MHz, Chloroform-*d*): δ (ppm) 7.77 (d, *J* = 8.2 Hz, 2H), 7.32 (d, *J* = 8.1 Hz, 2H), 4.16 – 4.13 (m, 2H), 3.68 – 3.65 (m, 2H), 3.55 (dd, *J* = 5.6, 3.5 Hz, 2H), 3.46 (dd, *J* = 5.6, 3.5 Hz, 2H), 3.32 (s, 3H), 2.42 (s, 3H).

3,4-Bis[2-(2-methoxyethoxy)ethoxy]benzaldehyde (2):

Into a 100-mL single-necked round-bottom flask were added 2-(2-methoxyethoxy)ethyl p-toluenesulfonate (1a, 8.00 g, 29.2 mmol), 3,4-dihydroxybenzaldehyde (2.00 g, 14.6 mmol), anhydrous potassium carbonate ($K_2CO_3$, 5.42 g, 39.2 mmol), and 32 mL anhydrous dimethylformamide (DMF). The reaction mixture was stirred at 70 °C under inert atmosphere (or open to air if acceptable) for 24 h. After cooling to room temperature, the mixture was poured into water and extracted several times with ethyl acetate (EA). The combined organic extracts were dried over $Na_2SO_4$, filtered, and concentrated under reduced pressure. The crude product was purified by column chromatography on silica gel, using pure EA as eluent. The desired product was obtained as a yellow liquid in 70% yield. ^{1}H NMR (400 MHz, Chloroform-*d*): δ (ppm) 9.82 (s, 1H), 7.44 (d, *J* = 1.8 Hz, 1H), 7.42 (s, 1H), 6.98 (d, *J* = 8.0 Hz, 1H), 4.23 (dt, *J* = 10.0, 4.9 Hz, 4H), 3.90 (dt, *J* = 6.4, 3.1 Hz, 4H), 3.73 (td, *J* = 4.8, 1.9 Hz, 4H), 3.56 (td, *J* = 4.5, 1.2 Hz, 4H), 3.38 (s, 6H).

**Synthesis of TPP-OEG (target porphyrin derivative)**

Under an inert atmosphere (argon), 5,10,15,20-tetra(4-(4-bromobutoxy)phenyl)porphyrin (150 mg, 0.12 mmol), diethylamine (180 mg, 2.46

mmol), anhydrous potassium carbonate (K$_2$CO$_3$, 51 mg, 0.37 mmol), and 9 mL dry DMF were placed in a 50-mL two-necked round-bottom flask. After stirring for 15 min at ambient temperature, the reaction mixture was heated to 65 °C and refluxed for 24 h. Upon completion, the reaction mixture was cooled to room temperature and then washed several times with ice water. The organic layer was extracted with dichloromethane (DCM), dried over anhydrous Na$_2$SO$_4$, filtered, and concentrated under reduced pressure. The crude product was first subjected to recrystallization from a chloroform/methanol mixture for preliminary purification. After filtration and drying, further purification was carried out by silica-gel column chromatography using ethyl acetate (EA) containing triethylamine (EA:Et$_3$N = 1:0.2 $v/v$) as the eluent. The purified compound was finally recrystallized again from a chloroform/methanol mixture, filtered and dried to afford a bright purple solid in 51% yield. ^{1}H NMR (500 MHz, Chloroform-$d$): δ (ppm) 8.86 (s, 8H), 7.80 (s, 4H), 7.73 (d, $J$ = 7.8 Hz, 4H), 7.28 (d, $J$ = 8.1 Hz, 4H), 4.50 (t, $J$ = 5.0 Hz, 8H), 4.33 (t, $J$ = 4.9 Hz, 8H), 4.09 (t, $J$ = 5.0 Hz, 8H), 3.94 (t, $J$ = 4.9 Hz, 8H), 3.91 – 3.89 (m, 8H), 3.77 – 3.74 (m, 8H), 3.70 – 3.68 (m, 8H), 3.54 – 3.52 (m, 8H), 3.47 (s, 12H), 3.29 (s, 12H), -2.80 (s, 2H). Mass (MALDI-TOF): Obs. 1158.92; Calcd. For C$_{84}$H$_{110}$N$_4$O$_{24}$, 1559.81.


## 1.2. Device Fabrication and Methods

Solar cell devices fabrication

The organic solar cell devices were fabricated with inverted structure of Glass/ITO/ETL(SnO$_2$, SnO$_2$/TPP or SnO$_2$/TPP-OEG)/Active Layer/HTL (MoO$_3$)/Ag. Customized patterned indium tin oxide (ITO) glass substrates were sequentially cleaned through ultrasonic treatments in detergent, deionized water, and isopropanol. Afterward, the substrates were then dried overnight in a 70°C oven for later use. Before device fabrication, the ITO substrates underwent a 3-minute UV-ozone treatment. Tin oxide (SnO$_2$) nanoparticles were then spin-coated onto the ITO at 3000 rpm for 30 seconds. Subsequently, the substrates were annealed in air on a hotplate at 150°C for 30 minutes and then transferred into a nitrogen-filled glove box. For porphyrin-modified SnO$_2$ electron transport layers, TPP or TPP-OEG was dissolved in tetrahydrofuran at a concentration of 1 mg/mL, and the solution was spin-coated onto

the upper layer of $SnO_2$ to form a film with a thickness of about 3-5 nm. The active layer solution of PM6:L8-BO (with a weight ratio of 1:1.2, dissolved in CF) with a total concentration of 15.4 mg ml$^{-1}$ was spin-coated onto the $SnO_2$ layer at 4000 rpm, achieving an optimal thickness of 100 nm. Subsequently, the active layers were thermally annealed at 90 °C for 5 minutes. Finally, a deposition process involving the thermal deposition of 8 nm $MoO_3$ and 100 nm Ag was conducted on all devices through a mask under a vacuum of approximately $1 \times 10^{-7}$ mbar. The devices had an effective area of 0.036 cm$^2$.

Quantum chemistry calculations

The optimization of the complex were performed in the ORCA 5.0.4 package at B3LYP-D3(BJ)/6-31G(d) level.[1] Grimme's DFT-D3 method was adopted for correcting van der Waals interactions.[2] Prior to constructing the interfacial complexes, the geometries of TPP and TPP-OEG molecules were fully optimized to obtain their lowest energy conformations. Geometry optimizations of the $SnO_2$ porphyrin complexes were then performed with full structural relaxation, allowing both the $SnO_2$ cluster and the organic molecules to reorganize freely upon adsorption. This approach enables an accurate description of adsorption induced structural reconstruction at the interface.

Based on the optimized geometries, The binding energies (E) were calculated at B3LYP-D3(BJ)/def2tzvp level by the following formula:

$$\Delta E_{bind} = E_{complex} - (E_{SnO2} + E_{TPP/TPP\text{-}OEG}) \tag{1}$$

Where $\Delta E_{bind}$ is the total energy of the complex, $E_{complex}$ is the total energy of TPP or TPPZn molecule, $E_{SnO2}$ is the the total energy of $SnO_2$. The interaction analysis of the complex was characterized by Reduced density gradient (RDG) method and the based isosurface maps were rendered by Visual Molecular Dynamics (VMD) 1.9.3 from the cube files exported from Multiwfn 3.8.[3-5]

## 1.3. Instruments and Characterization

Photovoltaic Performance

The photovoltaic performance of the solar cells was measured under AM1.5G irradiation (100 mW cm$^{-2}$) using a Class A solar simulator (Enlitech, Taiwan), calibrated with a single-crystal silicon reference cell certified by the China General Certification Center (Enlitech). Current density−voltage ($J$−$V$) curves were recorded with a Keithley 2400 source meter.

External Quantum Efficiency (EQE)

EQE spectra were obtained using a QE system (QE-R3011, Enlitech), with light intensity calibrated by a standard single-crystal silicon photovoltaic cell (Enlitech).

Space-Charge-Limited Current (SCLC) Measurements

Devices were fabricated with the following structures: ITO/PEDOT/Active layer/MoO$_3$/Ag for hole mobility and ITO/ETL(SnO$_2$, SnO$_2$/TPP or SnO$_2$/TPP-OEG)/Active layer/ZnO NPs/Ag for electron mobility. Charge carrier mobility was determined by fitting the dark current to a single-carrier SCLC model using the equation: $J = 9\varepsilon_0\varepsilon_r\mu V^2/8d^3$. Here, $J$ is the current density, $\varepsilon_r$ is the relative dielectric constant of the transport medium, $\varepsilon_0$ is the permittivity of free space, d is the active layer thickness, and $\mu$ is the charge carrier mobility. $V = V_{app} - V_{bi}$, where $V_{app}$ is the applied voltage and $V_{bi}$ is the built-in voltage. Carrier mobility was calculated from the slope of the $J^{1/2} \sim$ V curves.

Light-Intensity Dependence

Light-intensity dependence measurements were conducted under illumination with a photon flux between 10–100 mW cm$^{-2}$, calibrated with a standard single-crystal silicon solar cell (Enlitech). Current density and voltage were recorded using a Keithley 2400 source meter.

Transient Photocurrent (TPC) and Transient Photovoltage (TPV) Measurements

The TPC and TPV characteristics of the devices were measured by applying 500 nm laser pulses with a pulse width of 120 fs and low pulse energy to short-circuit devices

in the dark.

Surface energy

The surface energy of films was obtained by VCA15 surface contact angle analyzer (Data physics).

UV−vis−NIR absorption spectra

UV−vis−NIR absorption spectra of the donor, acceptor and porphyrin in CF solutions and as thin films were recorded on a SHIMADZU UV-3600 spectrophotometer. The concentration of diluted solution was $1.0 \times 10^{-5}$ M, and the films were prepared by spin coating their solutions on glass substrates.

Built-in potential measurement

Mott-Schottky characteristics were measured using a Keysight E4990A Vector Network Analyzer, with a voltage range of -3 to 2 V in dark conditions. Device performance was tested both before and after measurements, with no indication of degradation.

Electrochemical impedance spectroscopy (EIS)

Impedance characteristics were measured using a Keysight E4990A Vector Network Analyzer over a frequency range from 1 Hz to 10 MHz in the dark. Device performance was verified before and after measurements, showing no signs of degradation.

Capacitance–frequency characteristics (C-F)

The capacitance–frequency characteristics were examined using a Keysight impedance analyzer (model E4990A), in a frequency range from 20 to $10^7$ Hz, with a small oscillation amplitude of 20 mV. The DOS distribution is fitted using the equation of

$$g(E) = \frac{N}{\sqrt{2\pi}\sigma} exp\left[ -\frac{(E - E_t)^2}{2\sigma^2} \right]$$, where $g(E)$ represents the total trap density, $E_t$ is the center of the distribution of the trap density of state, and $\sigma$ is the disorder parameter.

Grazing incidence wide-angle X-ray scattering (GIWAXS)

The GIWAXS measurements were carried out with a Xeuss 2.0 SAXS/WAXS laboratory beamline S3 using a Cu X-ray source (8.05 keV, 1.54 Å) and a Pilatus3R 300K detector. The incidence angle is 0.2°.
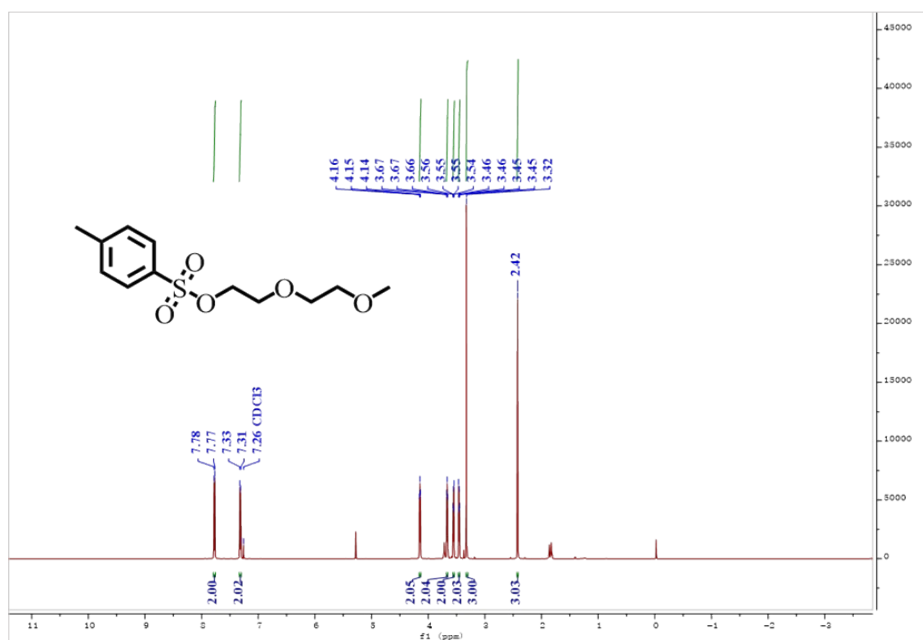
## 2. Supplementary Figures and Tables
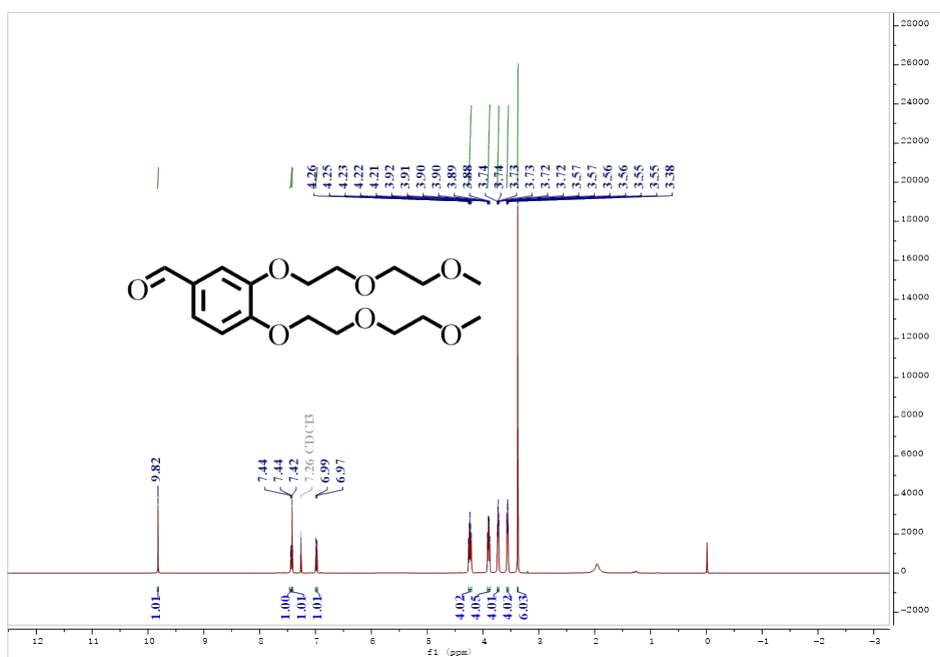


Fig. S1 $^1$H NMR (CDCl$_3$) spectrum of compound **1**.



Fig. S2 $^1$H NMR (CDCl$_3$) spectrum of compound **2**.
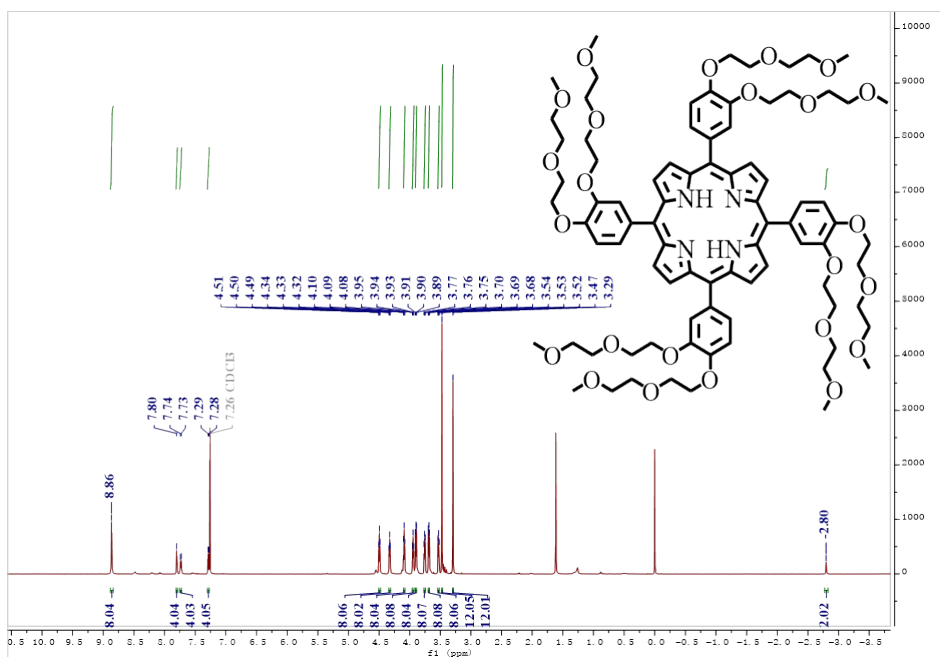
Fig. S3 ¹H NMR (CDCl$_3$+d5-Pyridine) spectrum of compound TPP-OEG.
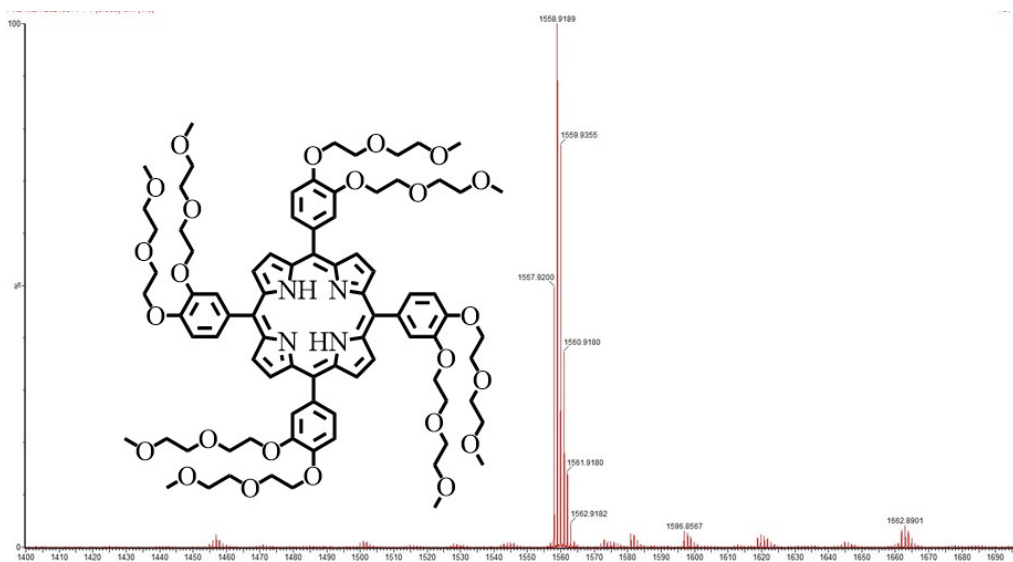


Fig. S4    Mass (MALDI-TOF) spectrum of TPP-OEG.

−0.045 eV <span>[color scale]</span> 0.045 eV
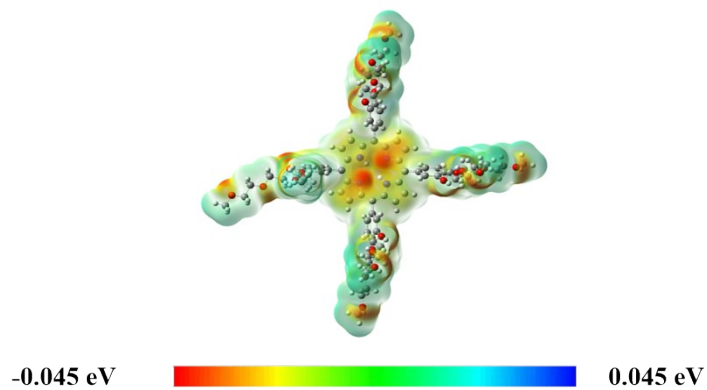
Fig. S5 Electrostatic potential distribution of TPP-OEG molecular.
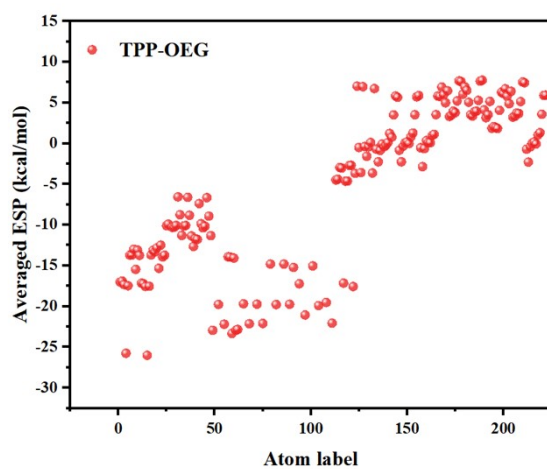


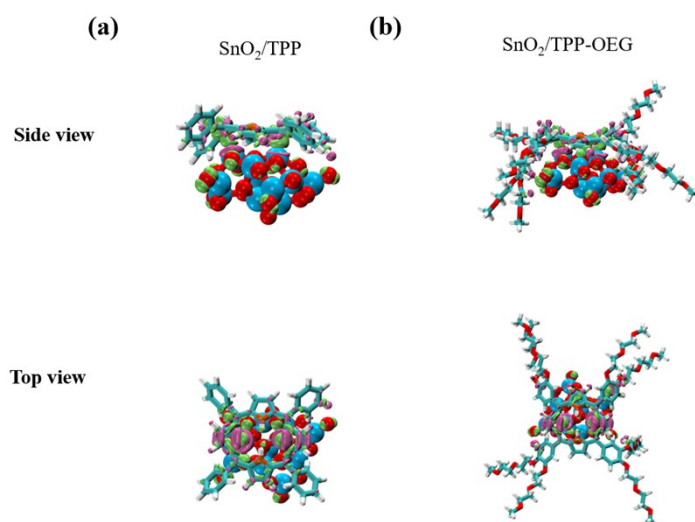Fig. S6 Average ESP statistics of each atom of the TPP-OEG model.



Fig. S7 Charge difference density (CDD) maps of (a) TPP and (b) TPP-OEG at $SnO_2$ substrate at the optimized geometry (The increase and decrease of electron density are noted in green and purple, respectively).
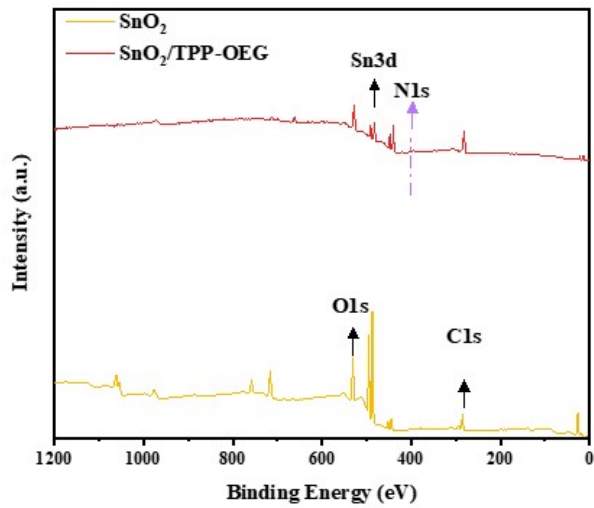
Fig. S8 X-ray photoelectron spectra (XPS) of $SnO_2$ and $SnO_2$/TPP-OEG films.
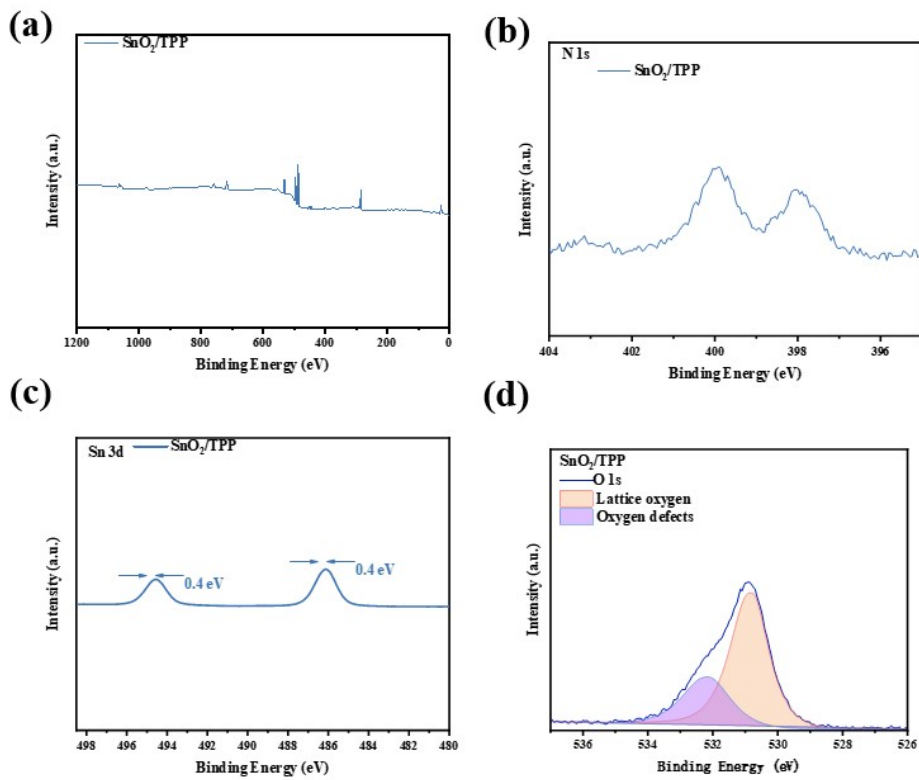


Fig. S9 X-ray photoelectron spectra (XPS) of $SnO_2$/TPP films.[6] Copyright 2025, Wiley-VCH.
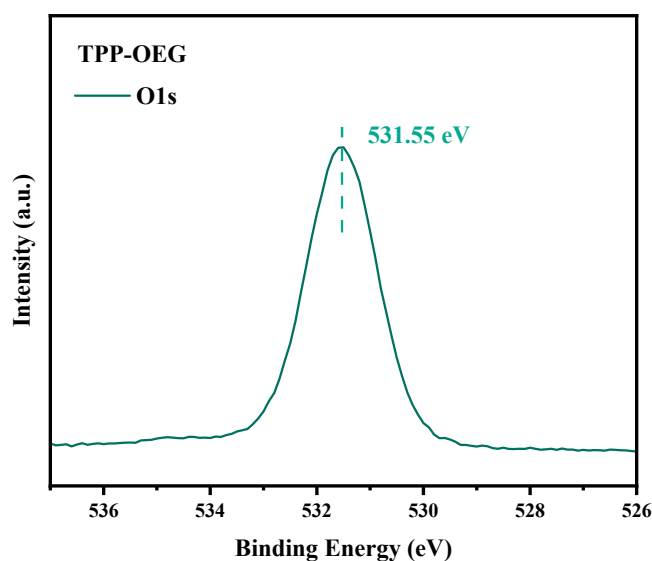
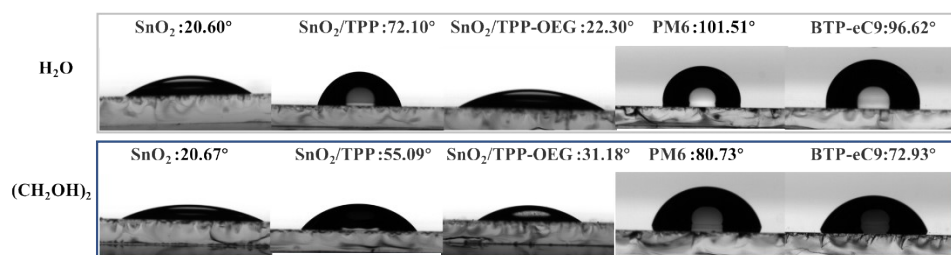Fig. S10 O 1s core level spectra of the TPP-OEG films.



Fig. S11 Water and ethylene glycol contact angles at the films of different ETLs and active layer materials.
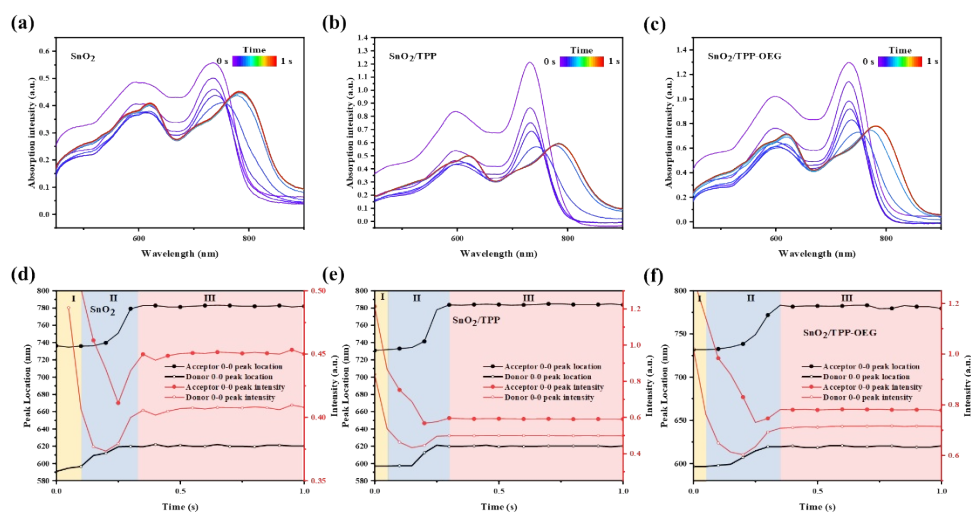


Fig. S12 (a-c) Time-resolved UV-vis absorption spectra and (d-f)The peak position evolution extracted from time-resolved UV-vis absorption spectra.
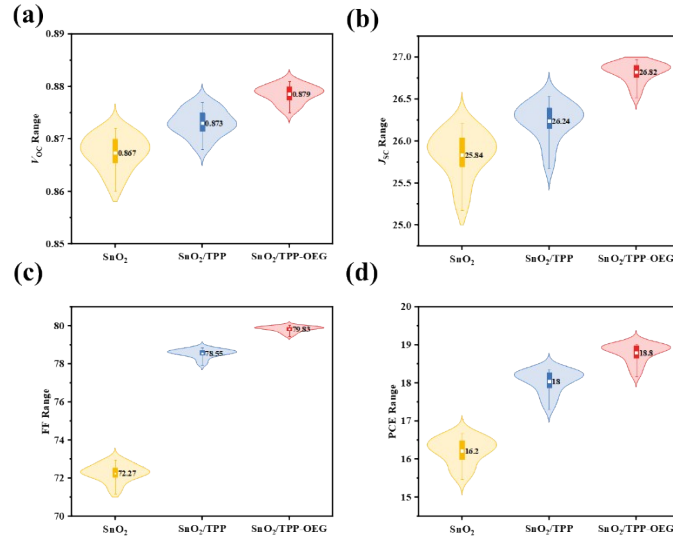
Fig. S13 Violin plots based on 20 independent devices for each ETL.
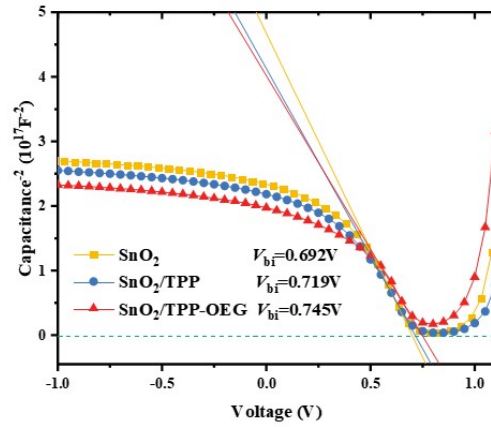


Fig. S14 Current-voltage (*C-V*) curves of the devices based on different ETLs under dark conditions.
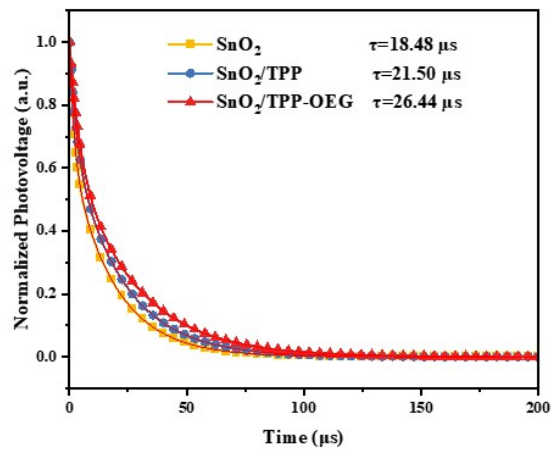


Fig. S15 Normalized transient photovoltage traces.
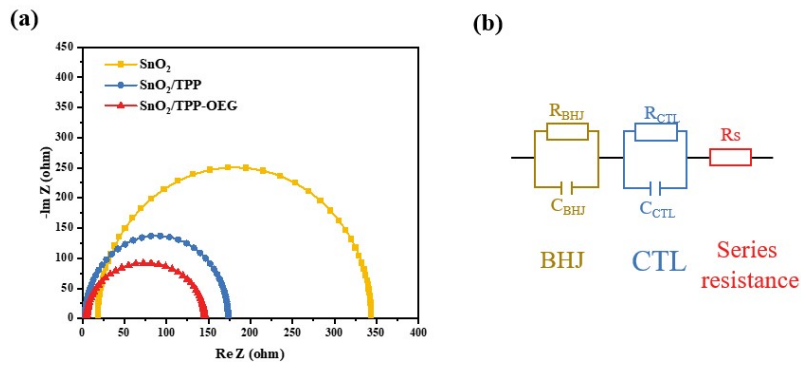
Fig. S16 Nyquist plot of the devices based on different ETLs and the equivalent-circuit model employed for EIS fitting.
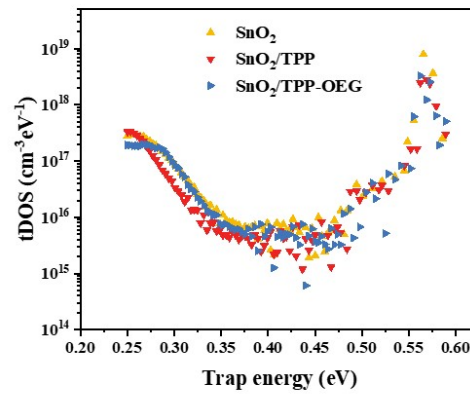


Fig. S17 The defects density of state (DoS) of devices based different methods measured following the Mott-Schottky method at 100 kHz in dark.
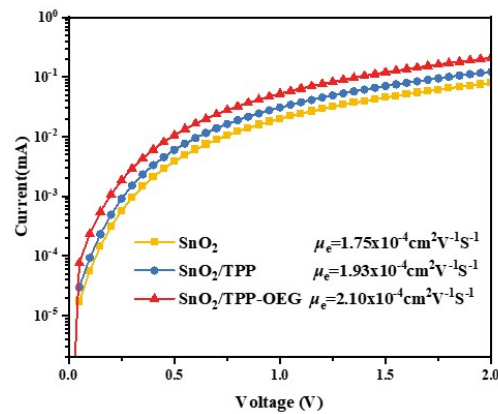


Fig. S18 $J-V$ curves of electron-only devices in a device structure of ITO/ETLs/PM6:L8-BO/ZnO NPs/Ag.
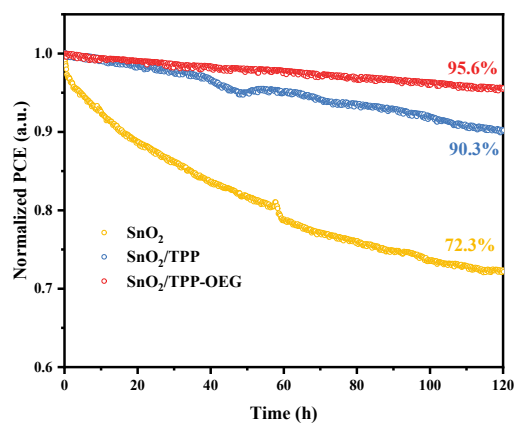
Fig. S19 Photo stability of three devices.



BTR-Cl                          PY-IT                          BTP-eC9
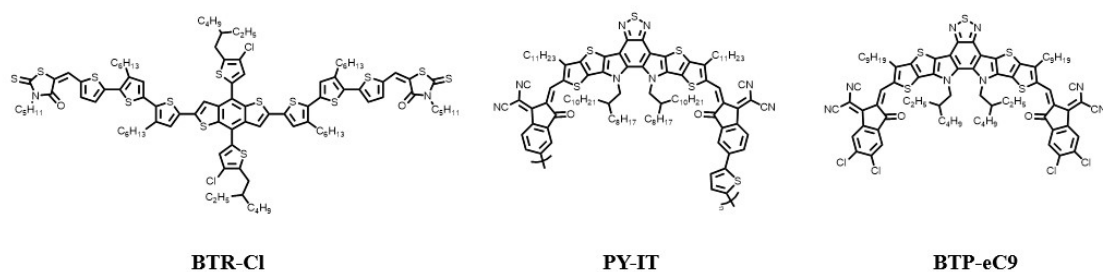
Fig. S20 Chemical structures of the donor and acceptors used in device fabrication.
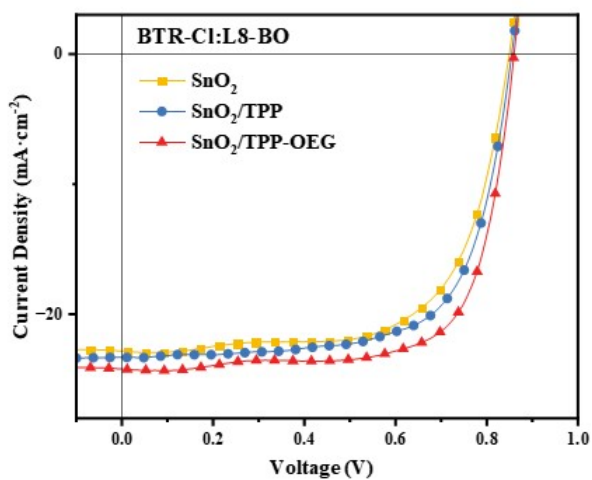


Fig. S21 *J–V* curves of the three devices with BTR-Cl:L8-BO active layer.
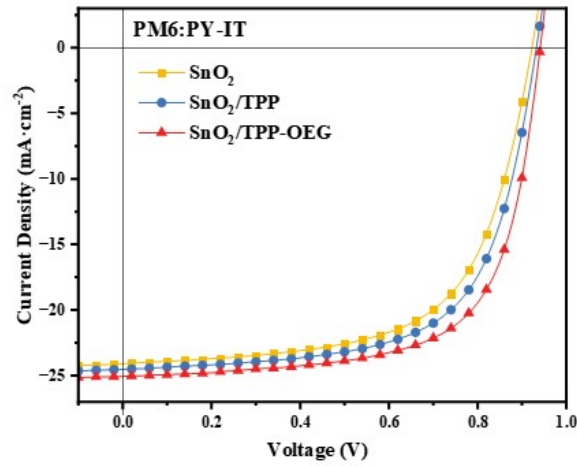
Fig. S22 *J–V* curves of the three devices with PM6:PY-IT active layer.

Table S1. The detailed parameters of corresponding 2D GIWAXS.

| ETL | | q (Å) | FWHM (Å) | CCL (nm) | d (Å) |
|---|---|---|---|---|---|
| SnO$_2$ | (0 1 0) Out of plane | 1.733 | 0.311 | 1.816 | 3.626 |
| | (1 0 0) In plane | 0.280 | 0.123 | 4.597 | 22.440 |
| SnO$_2$/TPP | (0 1 0) Out of plane | 1.734 | 0.301 | 1.877 | 3.624 |
| | (1 0 0) In plane | 0.282 | 0.118 | 4.792 | 22.281 |
| SnO$_2$/ TPP-OEG | (0 1 0) Out of plane | 1.736 | 0.285 | 1.982 | 3.619 |
| | (1 0 0) In plane | 0.283 | 0.117 | 4.833 | 22.202 |

**Table S2.** contact angle and surface free energy of ETL and active materials.

| ETL | $H_2O$ (°) | $(CH_2OH)_2$ (°) | $\gamma_S$ (mN·m⁻¹) | $\gamma_P$ (mN·m⁻¹) | $\gamma_D$ (mN·m⁻¹) |
|---|---|---|---|---|---|
| $SnO_2$ | 20.60 | 20.67 | 75.42 | 73.56 | 1.86 |
| $SnO_2$/TPP | 72.10 | 55.09 | 32.54 | 17.97 | 14.57 |
| $SnO_2$/TPP-OEG | 22.30 | 31.18 | 67.48 | 50.42 | 17.06 |
| PM6 | 101.51 | 80.73 | 17.71 | 2.28 | 15.43 |
| BTP-eC9 | 96.62 | 72.93 | 22.28 | 2.59 | 19.69 |

Table S3. The SCLC electron mobilities based on different ETLs and Hole mobility.

| ETL | $\mu_e$ (×10⁻⁴ cm²V⁻¹s⁻¹) | $\mu_h$ (×10⁻⁴ cm²V⁻¹s⁻¹) | $\mu_h/\mu_e$ |
|---|---|---|---|
| $SnO_2$ | 1.75 | 2.05 | 1.1714 |
| $SnO_2$/TPP | 1.93 | 2.05 | 1.0621 |
| $SnO_2$/ TPP-OEG | 2.10 | 2.05 | 0.976 |

Table S4. Photovoltaic parameters of devices with different ETLs and BHJs under AM 1.5G illumination at 100 mW·cm$^{-2}$.

| BHJ | ETLs | $V_{OC}$ (V) | $J_{sc}$ (mA·cm$^{-2}$) | FF (%) | PCE[b] (%) |
|---|---|---|---|---|---|
| BTR-Cl:L8-BO[a] | SnO$_2$ | 0.849 | 22.76 | 65.40 | 12.63 |
| | SnO$_2$/TPP | 0.855 | 23.49 | 68.49 | 13.75 |
| | SnO$_2$/TPP-OEG | 0.861 | 24.20 | 72.16 | 15.03 |
| PM6:PY-IT[b] | SnO$_2$ | 0.928 | 24.46 | 63.45 | 14.40 |
| | SnO$_2$/TPP | 0.938 | 25.13 | 68.97 | 16.25 |
| | SnO$_2$/ TPP-OEG | 0.944 | 25.65 | 70.32 | 17.02 |
| PM6:L8-BO: BTP-eC9[c] | SnO$_2$ | 0.884 | 26.35 | 76.34 | 17.78 |
| | SnO$_2$/TPP | 0.888 | 26.75 | 79.43 | 18.86 |
| | SnO$_2$/TPP-OEG | 0.893 | 27.10 | 80.98 | 19.60 |

[a] D:A = 1:1.4 (weight ratio); donor concentration = 7mg mL$^{-1}$ in CF with DIO as solvent additive (the volume of DIO is 0.7% of volume of CF), following with 80 ℃ TA treatment for 5 min. [b] D:A =1:1 (weight ratio); donor concentration = 7 mg mL$^{-1}$ in CF with CN as liquid additive (the volume of CN is 1% of volume of CF), following with 95 ℃ TA treatment for 5 min. [c] D1:A1:A2 = 1:1.1:0.1 (weight ratio); donor concentration = 6 mg mL$^{-1}$ in CF with DIO as solvent additive (the volume of DIO is 1% of volume of CF), following with 90 ℃ TA treatment for 5 min. The device structure is ITO/ETLs/active layer/MoO$_3$/Ag.

Table S5. PCE summary of a representative inverted OSCs.

| Year | ETL | Structures | BHJ | PCE (%) | Ref. |
|---|---|---|---|---|---|
| 2021 | ZnO | ITO/ZnO/PET/BHJ/MoO$_3$/Ag | PM6:Y6 | 16.46 | [7] |
| 2021 | ZnO | ITO/ZnO:Zr/BHJ/MoO$_3$/Ag | PM6:BTP-eC9 | 17.7 | [8] |
| 2021 | ZnO | ITO/PA-ZnO/BHJ/MoO$_3$/Ag | PM6:BTP-eC9 | 17.6 | [9] |
| 2022 | ZnO | ITO/ZnO/BHJ/MoO$_3$/Ag | PM6:Y6 | 15.03 | [10] |
| 2022 | CD | ITO/CD/BHJ/MoO$_3$/Ag | PM6:BTP-eC9 | 17.35 | [11] |
| 2022 | ZnO | ITO/ZnO/BHJ/MoO$_3$/Ag | PM6:N3 | 15.00 | [10] |
| 2022 | ZnO | ITO/ZnO/BHJ/MoO$_3$/Ag | PM6:ITIC | 10.28 | [10] |
| 2022 | ZnO | ITO/ZnO/PET/BHJ/MoO$_3$/Ag | PM6:L8-BO | 17.02 | [10] |
| 2022 | ZnO | ITO/ZnO/BHJ/MoO$_3$/Ag | PM6:IT-4F | 11.18 | [10] |
| 2022 | SnO$_2$ | ITO/SnO$_2$:PAS/BHJ/MoO$_3$/Ag | PM6:Y6 | 16.37 | [12] |
| 2022 | SnO$_2$ | ITO/SnO$_2$/1-DPAQ/BHJ/MoO$_3$/Ag | PM6:BTP-eC9 | 17.7 | [13] |
| 2022 | SnO$_2$ | ITO/SnO$_2$/1-DPAQ/BHJ/MoO$_3$/Ag | PM6:PB2F:BTP-eC9 | 18.1 | [13] |
| 2022 | SnO$_2$ | ITO/SnO$_2$:PAS/BHJ/MoO$_3$/Ag | PM6:BTP-eC9 | 17.12 | [12] |
| 2023 | ZnO | ITO/ZnO/PFN-Br/BHJ/Br-2PACz/MoO$_3$/Ag | PM6:PM7-Si:BTP-eC9 | 18.72 | [15] |
| 2023 | SnO$_2$ | ITO/SnO$_2$/Phen-NaDPO/BHJ/MoO$_3$/Ag | PM6:Y6 | 17.06 | [16] |
| 2023 | c-NDI | ITO/c-NDI:Pcy2/BHJ/MoO$_3$/Al | PM6:BTP-eC9 | 17.7 | [17] |
| 2023 | SnO$_2$ | ITO/SnO2/NMA/BHJ/MoO$_3$/Ag | PM6:L8-BO | 18.33 | [18] |
| 2024 | ZnO | ITO/DMF-ZnO/BHJ/MoO$_3$/Ag | PM6:BTP-eC9 | 18.14 | [19] |
| 2024 | ZnO | ITO/ZnO/ZrSe2/BHJ/MoO$_3$/Ag | PM6:L8-BO | 18.24 | [20] |
| 2024 | ZrO$_2$ | ITO/OSiNDs: ZrO$_2$/BHJ/MoO$_3$/Ag | PM6:BTP-eC9 | 18.43 | [21] |
| 2024 | ZnO | ITO/ZnO:PMMA/BHJ//MoO$_3$/Ag | PM6:D18:L8-BO | 18.72 | [22] |
| 2024 | InOx | ITO/ InOx/ZnO/BHJ/MoO$_3$/Ag | PM6:L8-BO:S10 | 19.06 | [23] |
| 2024 | SnO$_2$ | ITO/SnO$_2$/BHJ: Phen-NaDPO/MoO$_3$/Ag | PM6:D18:L8-BO | 18.87 | [24] |
| 2025 | ZnO | ITO/ZnO/VTMS/BHJ//MoO$_3$/Ag | PM6: BTP-eC9 | 18.92 | [25] |
| 2025 | SnO$_2$ | ITO/SnO$_2$/TPP-OEG/BHJ//MoO$_3$/Ag | PM6:L8-BO: BTP-eC9 | **19.60** | This work |

Table S6. Comparison between TPP-OEG and other modifiers in terms of efficiency, stability and cost.

| ETL | Active layer | efficiency | | | | stability | | cost |
|---|---|---|---|---|---|---|---|---|
| | | $J_{SC}$ [mA cm$^{-2}$] | $V_{OC}$ [V] | FF [%] | PCE [%] | Time | $PCE_t$/ $PCE_0$ | |
| SnO$_2$ | PTB7-Th: PC$_{71}$BM | 16.37 | 0.5 | 52.7 | 4.31 | - | - | 8,140.3 ¥/g （Merck） |
| SnO$_2$/ PFN | | 19.41 | 0.8 | 71.2 | 11.05 | - | - | |
| SnO$_2$ | PTB7-Th: PC$_{71}$BM | 16.71 | 0.69 | 47.68 | 5.49 | | 86.1% | - |
| SnO$_2$/ Li$_2$CO$_3$ | | 16.88 | 0.77 | 51.48 | 6.70 | 6 weeks [a] | 90.5% | 44.7 ¥/g （Merck） |
| SnO$_2$/ K$_2$CO$_3$ | | 16.85 | 0.77 | 52.91 | 6.85 | | 90.3% | 6.37 ¥/g （Merck） |
| SnO$_2$/ Rb$_2$CO$_3$ | | 16.89 | 0.78 | 55.55 | 7.35 | | 94.3% | 83.1 ¥/g （Merck） |
| SnO$_2$ | PM6:Y6 | 25.86 | 0.82 | 69.84 | 14.72 | 1000 hours [b] | 0.09% | - |
| SnO$_2$: PAS | | 26.01 | 0.85 | 74.04 | 16.37 | | 36.5% | 116.8 ¥/g （Merck） |
| SnO$_2$ | PM6: L8-BO | 26.21 | 0.872 | 72.98 | 16.23 | 1000 hours [c] | 91.8% | - |
| SnO$_2$/ TPP-OEG | | 26.97 | 0.881 | 80.03 | 18.84 | | 98.6% | 14.06 ¥/g （J&K） |

[a] stored in ambient air conditions without encapsulation; [b] under AM 1.5 standard sunlight for continuous irradiation; [c] dark storage at room temperature with encapsulation.

**References**

1.  M. J. Frisch, G. W. Trucks, H. B. Schlegel, G. E. Scuseria, M. A. Robb, J. R. Cheeseman, G. Scalmani, V. Barone, G. A. Petersson, H. Nakatsuji, X. Li, M. Caricato, A. V. Marenich, J. Bloino, B. G. Janesko, R. Gomperts, B. Mennucci, H. P. Hratchian, J. V. Ortiz, A. F. Izmaylov, J. L. Sonnenberg, Williams, F. Ding, F. Lipparini, F. Egidi, J. Goings, B. Peng, A. Petrone, T. Henderson, D.

Ranasinghe, V. G. Zakrzewski, J. Gao, N. Rega, G. Zheng, W. Liang, M. Hada, M. Ehara, K. Toyota, R. Fukuda, J. Hasegawa, M. Ishida, T. Nakajima, Y. Honda, O. Kitao, H. Nakai, T. Vreven, K. Throssell, J. A. Montgomery Jr., J. E. Peralta, F. Ogliaro, M. J. Bearpark, J. J. Heyd, E. N. Brothers, K. N. Kudin, V. N. Staroverov, T. A. Keith, R. Kobayashi, J. Normand, K. Raghavachari, A. P. Rendell, J. C. Burant, S. S. Iyengar, J. Tomasi, M. Cossi, J. M. Millam, M. Klene, C. Adamo, R. Cammi, J. W. Ochterski, R. L. Martin, K. Morokuma, O. Farkas, J. B. Foresman and D. J. Fox, *Journal*, 2016.

2.     S. Grimme, J. Antony, S. Ehrlich and H. Krieg, *J. Chem. Phys.*, 2010, **132**, 154104.

3.     E. R. Johnson, S. Keinan, P. Mori-Sánchez, J. Contreras-García, A. J. Cohen and W. Yang, *J. Am. Chem. Soc.*, 2010, **132**, 6498-6506.

4.     T. Lu and F. Chen, *J. Comput. Chem.*, 2012, **33**, 580-592.

5.     W. Humphrey, A. Dalke and K. Schulten, *J. Mol. Graph.*, 1996, **14**, 33-38.

6.     J. Wu, Y. Li, F. Tang, Y. Guo, H. Wu, L. Yuan, G. Liu, Z. He and X. Peng, *Adv. Funct. Mater.*, 2025, **35**, 2504623.

7.     Y. Han, H. Dong, W. Pan, B. Liu, X. Chen, R. Huang, Z. Li, F. Li, Q. Luo, J. Zhang, Z. Wei and C.-Q. Ma, *ACS Appl. Mater. Interfaces*, 2021, **13**, 17869-17881.

8.     X. Song, G. Liu, P. Sun, Y. Liu and W. Zhu, *J. Phys. Chem. Lett.*, 2021, **12**, 10616-10621.

9.     X. Liu, Z. Zheng, J. Wang, Y. Wang, B. Xu, S. Zhang and J. Hou, *Adv. Mater.*, 2022, **34**, 2106453.

10.    B. Liu, X. Su, Y. Lin, Z. Li, L. Yan, Y. Han, Q. Luo, J. Fang, S. Yang, H. Tan and C.-Q. Ma, *Adv. Sci.*, 2022, **9**, 2104588.

11.    Y. Dong, R. Yu, B. Zhao, Y. Gong, H. Jia, Z. Ma, H. Gao and Z. a. Tan, *ACS Appl. Mater. Interfaces*, 2022, **14**, 1280-1289.

12.    H. Gao, X. Wei, R. Yu, F.-Y. Cao, Y. Gong, Z. Ma, Y.-J. Cheng, C.-S. Hsu and Z. a. Tan, *Adv. Opt. Mater.*, 2022, **10**, 2102031.

13.    R. Yu, X. Wei, G. Wu, T. Zhang, Y. Gong, B. Zhao, J. Hou, C. Yang and Z. a.

Tan, *Energy Environ. Sci.*, 2022, **15**, 822-829.

14. Q. Huang, J. Jing, K. Zhang, Y. Chen, A. Song, Z. Liu and F. Huang, *J. Mater. Chem. A*, 2022, **10**, 23973-23981.

15. Y. Lin, Y. Zhang, A. Magomedov, E. Gkogkosi, J. Zhang, X. Zheng, A. El-Labban, S. Barlow, V. Getautis, E. Wang, L. Tsetseris, S. R. Marder, I. McCulloch and T. D. Anthopoulos, *Mater. Horizons*, 2023, **10**, 1292-1300.

16. J. Wu, F. Tang, S. Wu, Y. Li, L. Xiao, X. Zhu and X. Peng, *Adv. Energy Mater.*, 2024, **14**, 2302932.

17. Y. Yang, J. Wang, Y. Zu, Q. Liao, S. Zhang, Z. Zheng, B. Xu and J. Hou, *Joule*, 2023, **7**, 545-557.

18. Z. Suo, Z. Xiao, S. Li, J. Liu, Y. Xin, L. Meng, H. Liang, B. Kan, Z. Yao, C. Li, X. Wan and Y. Chen, *Nano Energy*, 2023, **118**, 109032.

19. S. Li, W. Chen, C. Shi, Y. Gong, K. Yang, L. Jiang, X. Lu, H. Xie, J. Yuan and Y. Zou, *Small*, 2024, **20**, 2405743.

20. H. Li, B. Yu and H. Yu, *Adv. Funct. Mater.*, 2024, **34**, 2402128.

21. M. Cui, Q. Rong, R. Wang, D. Ye, N. Li and L. Nian, *Small*, 2024, **20**, 2311339.

22. Z. Fu, J.-W. Qiao, F.-Z. Cui, R.-H. Gui, P. Lu, H. Yin, X.-Y. Du and X.-T. Hao, *Adv. Mater.*, 2024, **36**, 2413317.

23. M. I. Nugraha, Z. Ling, F. Aniés, R. E. A. Ardhi, M. Gedda, D. Naphade, L. Tsetseris, M. Heeney and T. D. Anthopoulos, *Adv. Mater.*, 2024, **36**, 2310933.

24. J. Wu, Y. Li, F. Tang, Y. Guo, G. Liu, S. Wu, B. Hu, Y. Fu, X. Lu, G. Lu, Z. He, X. Zhu and X. Peng, *Small*, 2024, **20**, 2404066.

25. S. Li, Z. Fu, W. Chen, X. Lu, J. Xiang, J. Zhang, K. Han, J. Yuan and Y. Zou, *ACS Appl. Mater. Interfaces*, 2025, **17**, 35652-35660.